ELSEVIER

Solid State Ionics 91 (1996) 93–99

SOLID STATE IONICS

Electrical and interfacial properties of a $Li_3Fe_2(PO_4)_3$ single crystal with silver electrodes

A.K. Ivanov-Schitz[a,*], J. Schoonman[b]

[a]*Institute of Crystallography, Leninsky pr. 59, Moscow 117333, Russia*

[b]*Laboratory for Applied Inorganic Chemistry, Delft University of Technology, P.O. Box 5045, 2600 Delft, The Netherlands*

Received 11 January 1995; revised 29 March 1996; accepted 30 April 1996

Abstract

Electrical conductivity and thermal properties of $Li_3Fe_2(PO_4)_3$ single crystals have been studied over a wide temperature range. The phase transformation detected at 483 K by DSC is accompanied by an anomaly of the conductivity for crystals oriented along the *b*-axis. The transition to the high-temperature fast ionic phase is observed at about 588 K for crystals oriented along [101] and [10$\bar{1}$] directions. The highest conductivity is observed for measurements perpendicular to the *b*-axis.

Keywords: Electrical conductivity; Interfacial impedance; Lithium iron phosphate; Lithium ion conductors; Solid electrolytes

1. Introduction

Among the materials exhibiting high ionic conductivity, lithium ion conductors with skeleton structures are very interesting. The solid electrolytes $Li_3M_2(PO_4)_3$ (M = Fe, Sc) have a three-dimensional, so-called mixed network $[M_2(PO_4)_3]^{3-}$, with lithium ions in the channels within this framework. The peculiarities of the crystal structure of lithium iron phosphate have been studied extensively [1], and it has been established that there are three polymorphic modifications, i.e. α-, β- and γ-phases.

The 3D-framework, made up of PO_4-tetrahedra and MO_6-octahedra, remains practically without change during the phase transitions. The main difference consists in the distribution of the lithium ions, which are located in crystallographic positions. Li^+-ions are weakly linked with framework ions, providing, at elevated temperatures, remarkably high values of ionic conductivity [1]. The best fast ionic conductors, such as $Na_3Zr_2Si_2PO_{12}$ (NASICON) and $Na_3M_2P_3O_{12}$ (M = Fe, Sc) [2–6], have crystal structures related to the present compounds with a mixed $[M_2(PO_4)_3]^{3-}$ framework.

Preliminary results of the impedance of the interface inert electrode (Au, Ag, C)/single crystalline $Li_3M_2(PO_4)_3$ over the frequency range from 1 to 10^6 Hz have been reported earlier [7]. In a more recent study [8], detailed impedance data of a $Li_3Fe_2(PO_4)_3$ single crystal along the [10$\bar{1}$] direction are discussed. The equivalent circuit used in the latter study was shown to have an additional parallel RC-branch, which was interpreted as being associated with either subgrain boundaries or the formation of a surface layer with properties different from those of the bulk.

The purpose of the present study is to present and

*Corresponding author.

PII S0167-2738(96)00415-8

discuss in detail the bulk properties of $Li_3Fe_2(PO_4)_3$ along different crystallographic directions, and interfacial impedances in the cell $Ag/Li_3Fe_2(PO_4)_3/Ag$ in a temperature range covering the phase transitions.

2. Experimental

Crystals of $Li_3Fe_2(PO_4)_3$ (LFP) were grown from the flux. The unit cell parameters are gathered in Table 1. Details of the crystal growth have been reported elsewhere [9,10], and here the crystal growth procedure is only outlined. $LiF–V_2O_5$ was used as a solvent and lithium fluoride played the role of both solvent and lithium source in the crystallization. $Li_3Fe_2(PO_4)_3$ single crystals were grown from the flux $Fe_2O_3–NH_4H_2PO_4–LiF–V_2O_5$ at temperatures ranging from 950 to 1100 K. $Li_3Fe_2(PO_4)_3$ crystals usually grow as yellowish-brown prisms, having perfect cleavage in two directions. The single crystals have good optical quality, are transparent, and sometimes contain inclusions of the flux. Usually micro-twinning is observed. The crystal used for conductivity measurements had a good habit. After orientation using the X-ray Laue technique, samples were cut as rectangular bars from high quality single cystals. Difficulties concerning the correct orientation are connected with a small difference between a and c unit cell parameters, as can be seen from Table 1. Here, the errors in orientation did not exceed 5 to 8° along any of the directions. Typical sample dimensions are $3 \times 3 \times 5$ mm^3. The bar sides were oriented perpendicular and parallel to the crystallographic b axis of the low-temperature monoclinic phase (space group $P2_1/n$).

The phase transition temperature for the single crystals was determined using DSC-12E (Mettler), interfaced to a personal computer. A sample mass of approximately 19 mg was used, which was sealed in an aluminum pan. The heating (cooling) rate was 5°C/min.

Table 1
Unit cell parameters of $Li_3Fe_2(PO_4)_3$

	α-phase 293 K	β-phase 513 K	γ-phase 573 K
Space group	$P2_1/n$	$P2_1/n$	Pcan
a (A°)	8.562(2)	8.588(1)	8.592(2)
b (A°)	12.005(3)	12.112(2)	12.129(2)
c (A°)	8.612(2)	8.638(1)	8.637(1)
γ (deg)	90.51(2)	90.12(2)	–

The electrical conductivity of the single crystals was obtained from a.c. impedance measurements with ionically blocking silver electrodes. Silver paste (trade mark 'Permacol') was applied as an electrode onto polished and cleaned sample surfaces. The impedance spectroscopy measurements were performed using a Solartron-1260 Frequency Response Analyzer in the frequency range from 0.1 to 10^7 Hz. The a.c. signal amplitude was usually kept at 10 mV (r.m.s.). No voltage dependence was observed for voltages from 10 to 40 mV, but the larger a.c. voltages did improve the signal-to-noise ratio.

All experiments were made along the [010], [101] and [10$\bar{1}$] directions of the crystal. An ambient of purified argon was used and data were recorded in the temperature range from 400 to 750 K, the temperature accuracy being within ±1°. Thermal equilibration was allowed to occur for at least 30 min at each temperature before the measurements were made.

The experimental data were analyzed using the program 'EQUIVCRT', written by Boukamp [11]. The equivalent circuits shown in Fig. 1 were used to fit the experimental impedance data. The admittance of the constant phase element (CPE) is given by

$$Y_p^* = Y_0(j\omega)^n, \quad 0 < n < 1.$$

The value χ^2 is the estimated standard deviation of the entire fit:

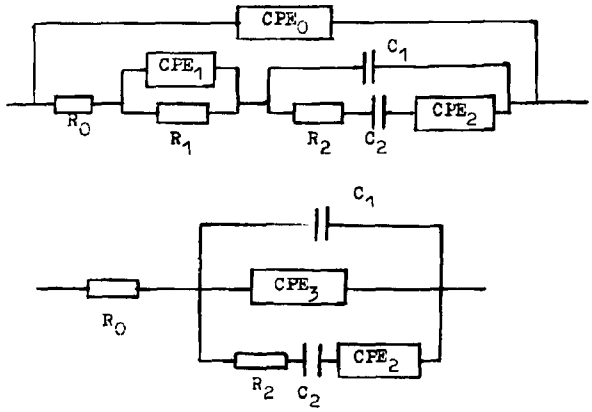

Fig. 1. Equivalent circuits for fitting of impedance data.

$$\chi^2 = \sum\{[Z'(\omega_i) - Z_i']^2 + [Z''(\omega_i) - Z_i'']^2\}/|Z(\omega_i)|^2.$$

Here, $Z'(\omega_i)$, $Z''(\omega_i)$ are the experimental values of the real and imaginary parts of the impedance determined at angular frequency ω_i, Z_i', Z_i'' are calculated values and $|Z(\omega_i)|^2 = [Z'(\omega_i)]^2 + [Z''(\omega_i)]^2$. With this program, the optimized component values for a wide variety of different equivalent circuit models could be rapidly evaluated. This procedure allows a comparison of alternative models and an evaluation of the physical interpretation of the components used in any given model.

In addition, d.c. polarization experiments, using the cell C/LFP/C indicated the electronic transference number to be smaller than 10^{-3} for all crystallographic directions. Therefore, a lithium ion contribution to the electrical conductivity dominates along all directions and for all temperatures studied.

3. Results and discussion

In general, the impedance spectrum can be rather complicated, as the total impedance may contain significant contributions from the bulk impedance, the twinning boundary impedance, a surface roughness effect, electrode polarization phenomena, diffusion of charge carriers and from the formation of poorly conducting surface layers.

Typical complex impedance plots for conduction along the different directions at low and high temperatures are shown in Figs. 2–4. It is seen that at low temperatures the impedance spectrum consists of four parts; a slightly depressed semi-circle, two partly overlapping depressed circles (or a fraction thereof; see Fig. 3a) and a straight line at low frequencies. As the temperature was increased, the resistive contributions decreased and the high-frequency semicircle disappeared. At high temperatures the impedance spectra practically reveal only the three latter parts and the semi-circles were found to decrease in size with increasing temperature.

The experimental impedance spectra were interpreted using equivalent circuits presented in Fig. 1. The circuit parameters will be discussed later. In order to obtain the bulk parameters, crystals with different sample lengths were investigated. It was found that the high-frequency, slightly depressed,

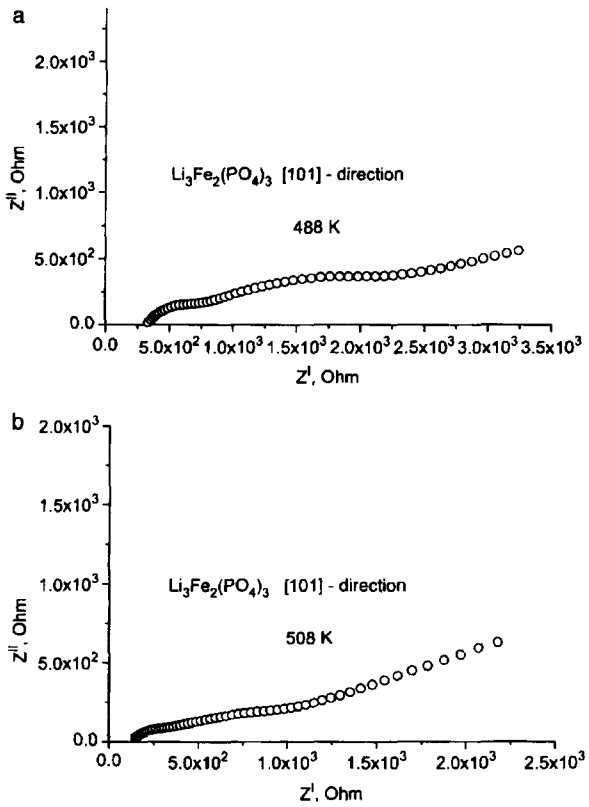

Fig. 2. Impedance of the cell $Ag/Li_3Fe_2(PO_4)_3/Ag$ measured along the [101] direction at 448 and 508 K in argon gas.

semi-circle (in the low temperature range, viz. Fig. 3a and Fig. 4a) corresponds to the bulk response, because the resistance term, R_0, is proportional to specimen thickness, and consequently, represents the bulk resistance. The parameter n of the circuit element CPE_0 is close to the ideal value of one for a perfect single crystal. For orientation along the b-axis the actual values range from 0.93 to 0.95 (Table 2). For a specimen, oriented along the [10$\bar{1}$] direction the values for n are smaller and varied from 0.64 to 0.91. It should be noted that at high temperatures the high-frequency arc, connected with the R_0CPE_0-branch, could not be measured (see Figs. 2 and 3b Fig. 4b).

After subtracting the R_0CPE_0-branch (or the R_0 resistance at high temperatures) two depressed and overlapping semi-circles remain in the impedance spectrum. These semi-circles are assumed to be related to different relaxation processes with close values for the time constants. The observed impe-

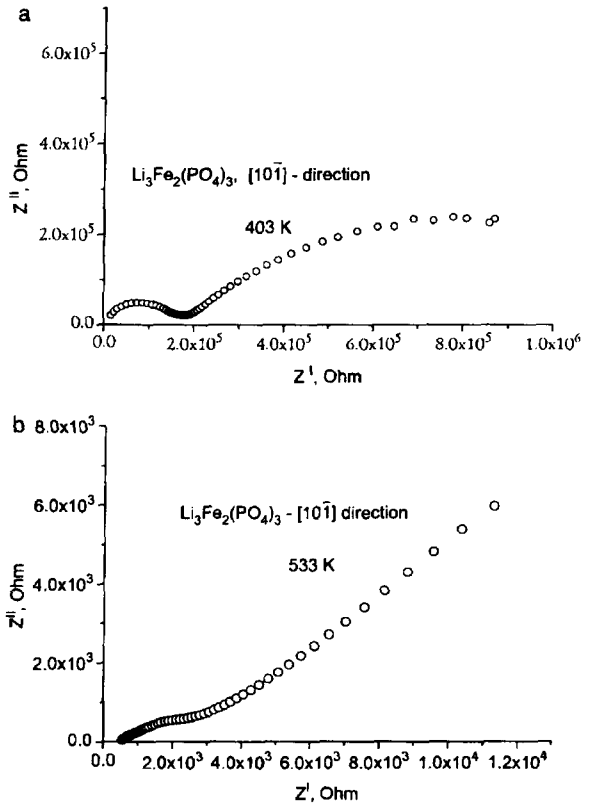

Fig. 3. Impedance of the cell $Ag/Li_3Fe_2(PO_4)_3/Ag$ measured along the [10$\bar{1}$] direction at 403 and 533 K in argon gas.

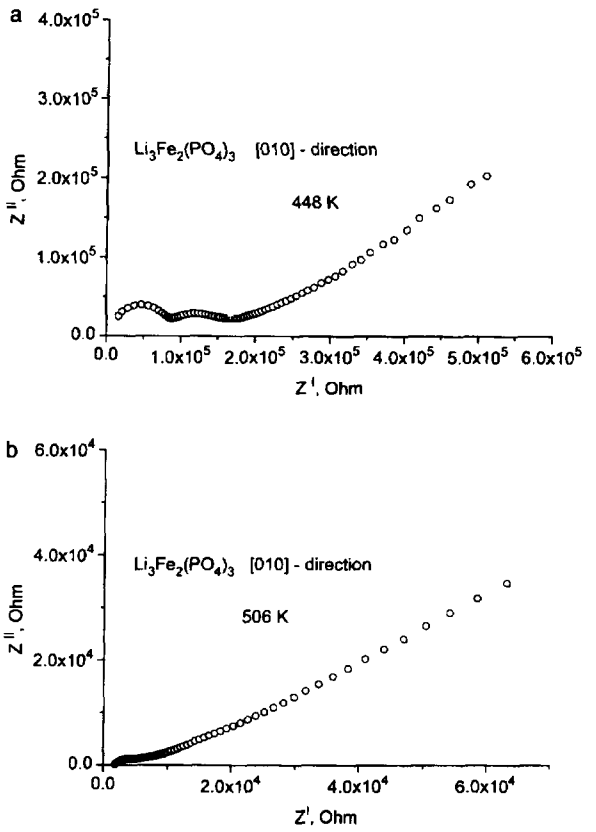

Fig. 4. Impedance of the cell $Ag/Li_3Fe_2(PO_4)_3/Ag$ measured along the [010] direction at 448 and 506 K in argon gas.

dance can be ascribed either to only electrode polarization phenomena, including a poorly conducting interface layer, or may include bulk relaxation processes. The experimental data obtained at $T<475$ K were consistent with the equivalent circuit presented in Fig. 1a.

From analyses of the impedance data for the sample, measured in all directions, it can be concluded that impedance spectra at temperatures above 500 K can be fitted using a slightly modified circuit, as presented in Fig. 1b.

4. Bulk properties

For a [010] oriented crystal at low temperatures, the value of the exponent n is close to unity, indicating the predominant capacitive nature of the CPE_0. Ignoring the deviation from an ideal capacitor, the CPE_0 element can be considered to be the geometrical capacitance. The data in Table 2 lead then to values of 45 to 70 for the dielectric constant. These values are much larger than the reported value of twelve for $Li_3Fe_2(PO_4)_3$ [12].

Plots of $\mathrm{Ln}(\sigma T)$ versus $10^3/T$ for different orientations of the crystal are given in Fig. 5. Two main features of the Arrhenius plot of $\sigma(T)$ should be noticed. Firstly, the anisotropy in the conductivity, the highest conductivity being observed for measurements perpendicular to the b-axis, and, secondly, a knee in the conductivity curves, which occurs at different temperatures for different directions. Concomitant changes in conductivity activation enthalpies ΔH_σ occur for [101] and [10$\bar{1}$] directions, while an increase in σ is first observed for the [010] direction. Moreover, the ΔH_σ value is always smaller in the high-conductivity phase. The transition to the high-temperature fast ionic phase is observed at about 588 K for measurements perpen-

Table 2
Fitting parameters of the low-temperature bulk impedance

[010]-direction				[10$\bar{1}$]-direction			
T (K)	R_0 (Ohm)	Y_0 (Mho)	n	T (K)	R_0 (Ohm)	Y_0 (Mho)	n
389	2.36×10^{6}	2.47×10^{-12}	0.96	365	4.35×10^{5}	4.83×10^{-12}	0.91
413	6.4×10^{5}	2.67×10^{-12}	0.95	403	1.19×10^{5}	4.72×10^{-11}	0.78
448	8.9×10^{4}	4.14×10^{-12}	0.93	443	1.94×10^{4}	5.76×10^{-10}	0.64

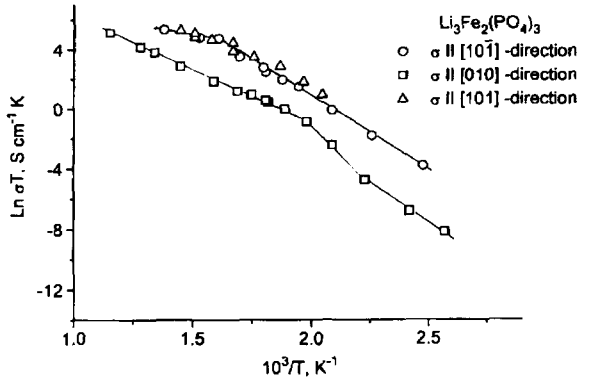

Fig. 5. Temperature dependencies of the conductivity of the $Li_3Fe_2(PO_4)_3$ single crystal.

dicular to the b-axis, and around 588 K the activation enthalpy decreases from 0.88 to 0.24 eV. The high-temperature anomaly around 480 K is observed for crystals oriented along the b-axis. The activation enthalpy changes from 0.84 to 0.58 eV.

As is apparent from the conductivity results presented in Fig. 5, the transition to the fast ionic state occurs at different temperatures. Recently, we have reported on the anomalous behavior of σ for LFP ceramics at about 450 and 560 K [9,13]. The Mössbauer spectra show the phase transitions to occur at about 463 and 523 K [14]. According to the results of an investigation of the conductivity and dielectric permittivity in the microwave range [12], there are two phase transitions at 483 and 523 K, respectively. These phase transformations are accompanied by a slight change of activation energy and a weak anomaly of σ. An anomalous decrease of the intensity of the 510 cm^{-1} band in the infrared spectra of LFP ceramics is observed with temperature [15]; the intensity is zero at 529 K. Similar results were obtained for Raman spectra; a steep decrease in the intensity of the 80 cm^{-1} band was observed at about 600 K [16]. The phase transition temperatures have been obtained by different techniques and are found in the ranges

$$\alpha\text{-LFP} \overset{480\text{–}513\ K}{\rightarrow} \beta\text{-LFP} \overset{570\text{–}600\ K}{\rightarrow} \gamma\text{-LFP}.$$

DSC experiments were used to investigate the $Li_3Fe_2(PO_4)_3$ single crystal employed for the conductivity measurements. The DSC curve is presented in Fig. 6. Only one endothermic peak is clearly oberved at about 483 K in the temperature range from room temperature to 800 K. The transition enthalpy is 0.8 kJ/mole. The temperature hysteresis is about 5–8 K. It should also be emphasized that the phase transition temperature, as obtained by DSC, is found in the range 468 to 490 K for different crystals and for crystals with different thermal histories [7]. The transition enthalpy is 0.7–1.3 kJ/mole.

The formation of the fast ionic state in $Li_3Fe_2(PO_4)_3$ may occur in two stages: firstly, the order–disorder transformation of the lithium sublattice occurs, followed by a heat peak on the DSC curve at 483 K and then the reorganization of the rigid oxide sublattice occurs with a change of the crystal symmetry at approximately 575 K. Apparently, disordering of the lithium sublattice promotes the

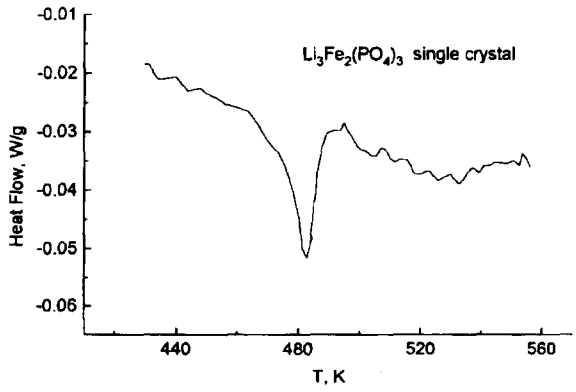

Fig. 6. DSC curve of a $Li_3Fe_2(PO_4)_3$ single crystal.

minor modification of the rigid skeleton. In conductivity measurements these effects are observed in different crystallographic directions. A decrease of the activation enthalpy in conductivity measured along the [101] and [10$\bar{1}$] directions can be qualitatively explained using the theory of defect exchange between inequivalent sites [17]. Analogous phenomena are observed for NASICON [18] and $Na_3Sc_2P_3O_{12}$ [19]. A detailed explanation for this effect cannot be given at present.

5. Interfacial response

The physical interpretation of the circuit parameters, except R_0CPE_0, of the equivalent circuits will be discussed here. The additional arc, described by R_1CPE_1 elements in the equivalent circuit of Fig. 1a, may be associated with the following processes, i.e. the crystal may contain some twinning boundaries, which are produced during crystal growth, or a poor conducting layer occurs on exposure of the crystal to air or due to a chemical surface reaction with the silver paste used as the electrode material. It has been reported [14], that twinning occurs in the low temperature α and β phases. These effects lead to a similar response as that of grain boundaries. The existence of a surface layer will affect the double layer area and hence the capacitance, which is associated with the mobile species. The formation of a surface layer with properties different from those of the bulk has been reported [20]. In the present case, the existence of the twinning boundaries as a result of polydomain structure formation seems to be the most probable. Above the phase transition temperature the equivalent circuit in Fig. 1b (without CPE_1R_1 branch) has been used. The equivalent circuit in Fig. 1b was used firstly by Macdonald [21] to fit the impedance data for a Li_3N crystal. It seems that C_1–R_2C_2–CPE_2–CPE_3 branches correspond to the processes at the Ag–$Li_3Fe_2(PO_4)_3$ interface, because there is no CPE_2 element for data obtained for impedance measurements in dry air. The capacitance, C_1, is now associated with accumulation of the lithium ions. The R_2–CPE_2–C_2 branch must be due to phenomena in the space charge region. While the detailed mechanism is not yet known, it is believed that diffusion of minority carriers and relaxation of the twinning boundaries may be involved [22,23]. The temperature curves for C_1 are presented in Fig. 7.

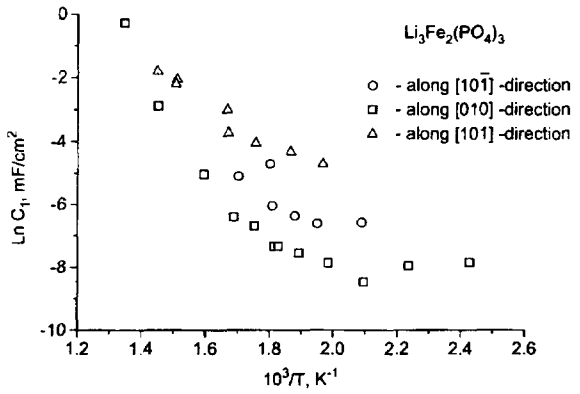

Fig. 7. The temperature dependencies of the C_1 capacitance for the impedance of the Ag–$Li_3Fe_2(PO_4)_3$ interface.

Acknowledgments

The authors are grateful to Dr. V.A. Timofeeva for the single crystals. One of the authors (A.K.I.-S.) would like to thank Dr. J. Schram for assistance in impedance data analysis and Eng. R. van Landschoot for technical assistance.

One of us (A.K.I.-S.) thanks the Russian Foundation for Basic Research for financial support (Grant No. 93-03-18310).

References

[1] A.B. Bykov, A.P. Chirkin., L.N. Demyanets, S.N. Doronin, E.A. Genkina, A.K. Ivanov-Schitz, I.P. Kondratyuk, B.A. Maksimov, O.K. Mel'nikov, L.A. Muradyan, V.I. Simonov and V.A. Timofeeva, Solid State Ionics 38 (1990) 31.

[2] B.I. Lazoryak, V.B. Kalinin, S.Yu. Stefanovich and V.A. Efremov, Dokl. Akad. Nauk SSSR 250 (1980) 861 (in Russian).

[3] V.A. Efremov and V.B. Kalinin, Sov. Phys. Crystall. 23 (1978) 703 (in Russian).

[4] H.Y.P. Hong, Mat. Res. Bull. 11 (1976) 173.

[5] M. Pintard-Screpel, F. d'Yvoire and E. Bretey, in: Proc. Second European Conference on Solid State Chemistry, Veldhoven, eds. R. Metselaar, H.J.M. Heijligers and J. Schoonman. 3 (1983) p. 264.

[6] F. d'Yvoire, M. Pintard-Screpel, E. Bretey and M. de la Rochere, Solid State Ionics 9/10 (1983) 851.
[7] A.K. Ivanov-Schitz, in: Elektrodika tverdotel'nych system, ed. M.V. Perfil'ev (Nauka, Sverdlovsk, 1991), p. 70 (in Russian).
[8] A.K. Ivanov-Schitz, V.A. Timofeeva and J. Schoonman, Elektrochimiya 30 (1994) 955 (in Russian).
[9] A.B. Bykov, L.N. Dumyanets, S.N. Doronin, A.K. Ivanov-Schitz, O.K. Mel'nikov, B.K. Sevastyanov, V.A. Timofeeva and A.P. Chirkin, Sov. Phys. Crystall. 32 (1987) 1515 (in Russian).
[10] A.B. Bykov, L.N. Demyanets, S.N. Doronin, A.K. Ivanov-Schitz, O.K. Mel'nikov, B.K. Sevastyanov, V.A. Timofeeva and A.P. Chirkin, Rost Krystallov 16 (1988) 44 (in Russian).
[11] B.A. Boukamp, Solid State Ionics 20 (1986) 31.
[12] A.S. Orlukas, A.K. Schukauskas, A.K. Ivanov-Schitz, S.B. Auksyalis, A.P. Keschenis, V.V. Styapankavichus, R.A. Mizeris, V.F. Mikuchyonis and R.A. Vaitkus, Lituv. Fiz. Sbornik 29 (1989) 689 (in Russian).
[13] E.A. Genkina, L.N. Demyanets, A.K. Ivanov-Schitz, B.A. Maksimov, O.K. Mel'nikov and V.I. Simonov, Pis'ma GETF 38 (1083) 257 (in Russian).
[14] I.P. Kondratyuk, B.A. Maksimov and L.A. Muradyan, Dokl. Akad. Nauk SSSR 292 (1987) 1376 (in Russian).
[15] V.V. Kravchenko, V.I. Michailov and S.E. Sigaryov, Solid State Ionics 50 (1992) 19.
[16] V.I. Michailov, B.N. Mavrin, A.K. Ivanov-Schitz and S.E. Sigaryov, Sov. Phys. Crystall. 37 (1992) 760 (in Russian).
[17] D.R. Franceschetti and P.C. Shipe, Solid State Ionics 11 (1984) 285.
[18] L.O. Atovmyan, N.G. Bukun and E.A. Ukshe, Elektrokhimiya 19 (1983) 933 (in Russian).
[19] N.G. Bukun, Materials Science Forum 76 (1991) 183.
[20] W.B. Reid and A.R. West, Solid State Ionics 45 (1991) 239.
[21] J.R. Macdonald, Solid State Ionics 58 (1992) 97.
[22] E.A. Ukshe and N.G. Bukin, Elektrokhimiya 26 (1990) 1373 (in Russian).
[23] M.G.S.R. Thomas, P.G. Bruce and J.B. Goodenough, J. Electrochem. Soc. 132 (1985) 1521.